Direct numerical simulations of particle collisions on a wet surface

DIRECT NUMERICAL SIMULATIONS OF PARTICLE COLLISIONS ON A WET SURFACE

Yali Tang[1], Britta Buck[2], Stefan Heinrich[2], Niels G. Deen[3], J.A.M. Kuipers[1]

1 Multiphase Reactors Group, Department of Chemical Engineering and Chemistry, Eindhoven University of Technology, P.O. Box 513, 5600 MB Eindhoven, NL
2 Institute of Solids Process Engineering and Particle Technology, Hamburg University of Technology, Denickestrasse 15, 21073 Hamburg, G
3 Multiphase and Reactive Flows Group, Department of Mechanical Engineering, Eindhoven University of Technology, P.O. Box 513, 5600 MB Eindhoven, NL
Corresponding E-mail: y.tang2@tue.nl

ABSTRACT

Direct numerical simulations can provide detailed understanding of micro-mechanics of individual particle collisions in the presence of liquid, which is crucial in wet granular flows in many industrial applications. In this work, a numerical model is developed for such detailed simulations of collision of a spherical particle on a wet surface. The model combines the immersed boundary method and the volume-of-fluid method supplemented with a contact model for the description of gas-liquid-solid contact line. Careful verifications of the model are conducted for droplet-wall as well as droplet-sphere contacts. Simulation results for normal collisions of a sphere on wet surfaces are reported, and compared with the corresponding experimental data.

KEYWORDS

VOF-IBM, wet restitution coefficient, direct numerical simulation, contact model

1. INTRODUCTION

In prevalent chemical and pharmaceutical industrial processes (such as filtration, coagulation, agglomeration, spray coating, drying, and pneumatic transport), liquid is intentionally injected either as a reactant or for coating purposes, resulting in wet particles (i.e., particles coated with a thin liquid layer). When interacting with each other or colliding with a wall, the wet particles impact and rebound in a completely different way from dry particles. This is due to the effects of the interstitial lubricating liquid, which changes the collisions [1]. If the liquid has a comparable density to the solid particles, the fluid motion and its non-negligible viscous effects introduce additional mechanisms for momentum and mass transport, as well as energy dissipation [2]. To accurately predict the behaviour of particulate flows involving liquid injection, a fundamental understanding of the influence of the liquid on the collision mechanism is crucial.

Considering the collision between a particle and a surface covered with a thin liquid layer, the impact characteristics are extremely complex due to the formation, extension and rupture of a liquid bridge during the rebound of the particle. Analogous to dry collisions, the description of wet collisions employs a so-called "wet restitution coefficient" e_{wet}, which accounts for the combined effects of the interstitial fluid (added mass, viscous dissipation, compressibility, etc.) and the inelasticity of the contact. It describes the energy dissipation E_{diss} of the system during a collision with initial kinetic energy E_{kin}, and is defined as:

$$e_{wet} = \frac{v_R}{v_{im}} = \sqrt{1 - \frac{E_{diss}}{E_{kin}}}\ , \qquad Eq\ (1)$$

where v_R and v_{im} are, respectively, the rebound velocity after the rupture of liquid bridge and the impact velocity when just touching the liquid layer. Many researches (e.g., [3-10]) have been conducted for the quantification/measurement of the e_{wet} in wet collision systems. However, numerical modelling, especially detailed numerical simulation (DNS) of such collision problems (e.g. [11]) is very limited. The difficulty lies in the complexity of solving a gas-liquid-solid three phase flow as well as its interface. Recent progress has been made by Wu et al. [12] and Kan et al. [13] on the prediction of dynamic liquid bridge with use of direct numerical simulations. Such progress demonstrates that DNS can be a potential and promising approach for further investigation of wet collision mechanisms. Therefore, in this work, a DNS model will be introduced, which not only can qualitatively reproduce the experimentally observed phenomena, but also can quantitatively predict the wet restitution coefficient for different collision scenarios of spheres impacting on wet surfaces.

2. METHODS

Our model consists of two main parts: one part deals with the presence of deformable by a volume-of-fluid (VOF) method, whereas the other part accounts for the presence of the solid particles taking into account the possible non-ideal particle-particle or particle-wall collisions by an immersed boundary method (IBM). The gas-liquid-solid interface and the wetting is modelled by integrating a contact model into the surface tension model in VOF.

2.1 Volume-of-fluid method

The VOF method is used to track the interface in two-material fluid flow involving two immiscible fluids. For incompressible multi-material flows the Navier-Stokes equations can be combined into a single equation for the fluid velocity $\boldsymbol{u}$ in the entire domain of interest (including the interior of the solid particles) taking into account surface tension through a local volumetric surface tension force $\boldsymbol{f}_\sigma$ (with dimensions N/m^3) accounting for the presence of curved deformable interfaces. The governing conservation equations for unsteady, incompressible, Newtonian, multi-fluid flows are given by the following expressions:

$$\nabla \cdot \boldsymbol{u} = 0\,, \qquad \textit{Eq (2)}$$

$$\rho\left(\frac{\partial \boldsymbol{u}}{\partial t} + \nabla \cdot \boldsymbol{u}\boldsymbol{u}\right) = -\nabla p + \rho \boldsymbol{g} + \nabla \cdot \mu\left((\nabla \boldsymbol{u}) + (\nabla \boldsymbol{u})^T\right) + \boldsymbol{f}_\sigma\,, \qquad \textit{Eq (3)}$$

where the local average density ρ and viscosity μ are evaluated respectively by linear and harmonic averaging of the densities of gas (g) phase and liquid (l) phase:

$$\rho = F\rho_l + (1-F)\rho_g\,, \qquad \textit{Eq (4)}$$

$$\frac{\rho}{\mu} = F\frac{\rho_l}{\mu_l} + (1-F)\frac{\rho_g}{\mu_g}\,, \qquad \textit{Eq (5)}$$

depending on the local distribution of the phase indicator or colour function F, which is governed by the given expression:

$$\frac{DF}{Dt} = \frac{\partial F}{\partial t} + \boldsymbol{u} \cdot \nabla F = 0\,. \qquad \textit{Eq (6)}$$

The Navier-Stokes equations are solved with a standard finite volume technique on a staggered rectangular 3D grid using a two-step projection-correction method. When the velocity field is calculated, the phase fraction can be updated by geometrical advection based on the interface reconstruction using the Piecewise Linear Interface Calculation (PLIC) algorithm of Youngs [14].

The volumetric surface tension force $\boldsymbol{f}_\sigma$ appearing in the momentum Eq. (3) only acts in the vicinity of the interface. The calculation of $\boldsymbol{f}_\sigma$ is based on the tensile force (TF) model, details of which can be found in Baltussen [15]. The TF model determines the surface force from tensile forces exerted on each interface element *m*, which is given by the following expression:

$$\boldsymbol{f}_{\sigma,m} = \frac{1}{2}\sigma \sum_i \boldsymbol{t}_{i,m} \times \boldsymbol{n}_i \,. \qquad \textit{Eq (7)}$$

The force direction is determined using the cross product of the normal of the neighbouring element $\boldsymbol{n}_i$ and the tangent $\boldsymbol{t}_{i,m}$ between the interface element *m* and its neighbouring elements *i*. σ is the surface tension coefficient. The tangent is created from the interface reconstruction, obeying the right-hand rule. The normal is calculated from the phase fraction using

$$\boldsymbol{n} = \frac{\nabla F}{|\nabla F|} \,. \qquad \textit{Eq (8)}$$

However, different treatment is needed at the gas-liquid-solid three-phase contact line. Thus, a contact model is included through the contact angle θ:

$$\hat{\boldsymbol{n}} = \boldsymbol{n}_s \cos\theta + \boldsymbol{t}_s \sin\theta \,, \qquad \textit{Eq (9)}$$

where $\hat{\boldsymbol{n}}$ is the unit vector normal to the contact surface, $\boldsymbol{n}_s$ and $\boldsymbol{t}_s$ represent the unit vector normal and tangent to the solid surface, respectively. The contact angle can be equilibrium contact angle θ_{eq}.

2.2 Immersed boundary method

The translational $\boldsymbol{v}_p$ and rotational $\boldsymbol{\omega}_p$ motion of the suspended solid particles is given by the Newtonian equations of motion, respectively, given by:

$$m_p \frac{d\boldsymbol{v}_p}{dt} = m_p \boldsymbol{g} + \boldsymbol{F}_{p,w}^{lub} + \boldsymbol{F}_{f\to s} \,, \qquad \textit{Eq (10)}$$

$$I_p \frac{d\boldsymbol{\omega}_p}{dt} = \boldsymbol{T}_{f\to s} \,, \qquad \textit{Eq (11)}$$

where m_p and I_p represent, respectively, the mass and the moment of inertia of the particle, $\boldsymbol{F}_{f\to s}$ and $\boldsymbol{T}_{f\to s}$ account for the liquid-solid interaction (respectively, drag and torque), and $\boldsymbol{F}_{p,w}^{lub}$ represents the lubrication force between particle and wall. The evaluation of the liquid-solid interaction is based on the second-order immersed boundary method by Deen et al. [16], where the details can be found. The unique feature of this coupling technique is the direct (i.e., implicit) incorporation of the no-slip boundary condition (Eq. (12)) at the surface of the particles at the level of the discrete momentum equations of the fluid. The no-slip boundary condition reads as:

$$\boldsymbol{u}_{particle-surface} = \boldsymbol{v}_p + \boldsymbol{\omega}_p \times \left(\boldsymbol{r} - \boldsymbol{r}_p\right), \qquad \textit{Eq (12)}$$

where $\left(\boldsymbol{r} - \boldsymbol{r}_p\right)$ is the distance between a certain point on the particle and the mass centre of the particle.

Dissipative particle-particle and/or particle-wall collisions are accounted via a hard sphere discrete particle approach. With respect to the specific flow problem considered in this work, a lubrication model is applied on the basis of the lubrication theory of Brenner [17]. For particle-wall interactions, the lubrication force reads as:

$$\boldsymbol{F}_{p,w}^{lub} = \begin{cases} 0, & 2h < \xi_{p,w} \\ -\frac{3\pi v_p \rho_l g}{2\xi_{p,w}} d_p^2 \boldsymbol{n}_w, & \xi_{min}^{lub} \le \xi_{p,w} \le 2h \\ 0, & \xi_{p,w} < \xi_{min}^{lub} \end{cases} \qquad \textit{Eq (13)}$$

where d_p is the particle diameter and $\boldsymbol{n}_w$ is the unit vector normal to the wall. Note that we only consider the normal component of the lubrication force, with respect to normal collisions in this work. For a surface distance, $\xi_{p,w}$between the particle and the wall, larger than two grid sizes 2*h*, the particle motion is resolved by the IBM and no modelling of the particle-wall interaction is required. When the particle approaches closer to the wall, the particle is more and more decelerated by the increasing pressure in the gap between the particle and the wall. Only if the surface distance becomes smaller than 2*h*, does the lubrication model set in till dry particle-wall contact (by hard sphere model) takes place. A cut-off distance ξ_{min}^{lub} is added to mimic real particles and prevent the lubrication force from reaching its singularity at zero normal distance. For the glass particles used in this work, we have set this cut-off distance as the particle roughness, thus $\xi_{min}^{lub} = 0.0001 d_p$.

3. VERIFICATION

The VOF and IBM has been extensively verified for gas-liquid systems (e.g. [15]) and fluid-solid systems (e.g., [16]), respectively. Here we would like to present further verification with respect to three-phase systems.

3.1 Droplet-wall contact

The evolution of a liquid droplet towards its static equilibrium in contact with a plane wall is modelled to test the implementation of the contact model. Starting from a perfectly spherical shape shown in Figure 1(a), the droplet motion is computed till its shape stabilizes. No gravity is considered, the droplet is therefore subjected to viscosity, inertia and surface tension including wall adhesion (via Eq. (9) with a given θ_{eq}). The simulated problem is similar to the work in Bellet et al. [18], except for the fluid properties, which are listed in Table 1. The resolution is kept the same for all the simulations, i.e., 20 grid cells per initial droplet diameter.

Table 1. Parameters used in simulation of droplet-wall contact.

Parameters	Values	Units
Liquid density ρ_l	1000	kg/m3
Liquid viscosity μ_l	0.001	Pa·s
Surface tension coefficient σ	0.073	N/m
Gas density ρ_g	1.2	kg/m3
Gas viscosity μ_g	1.8E-5	Pa·s
Droplet initial diameter	0.001	m

Different values of the equilibrium contact angle ($\theta_{eq} = 150°, 120°, 90°, 60°, 30°$) have been considered, with the stabilized droplet shape shown in Figure 1(b)-(f), respectively. Knowing θ_{eq}, the analytical solution of the height of the stable configuration can also be determined. The analytical solutions are compared to the simulation results in Figure 2. Both Figure 1 and Figure 2 indicate that our model can reproduce the analytical solutions to such droplet-wall contact problem at non-wetting ($\theta_{eq} > 90°$) as well as wetting ($\theta_{eq} \leq 90°$) conditions.

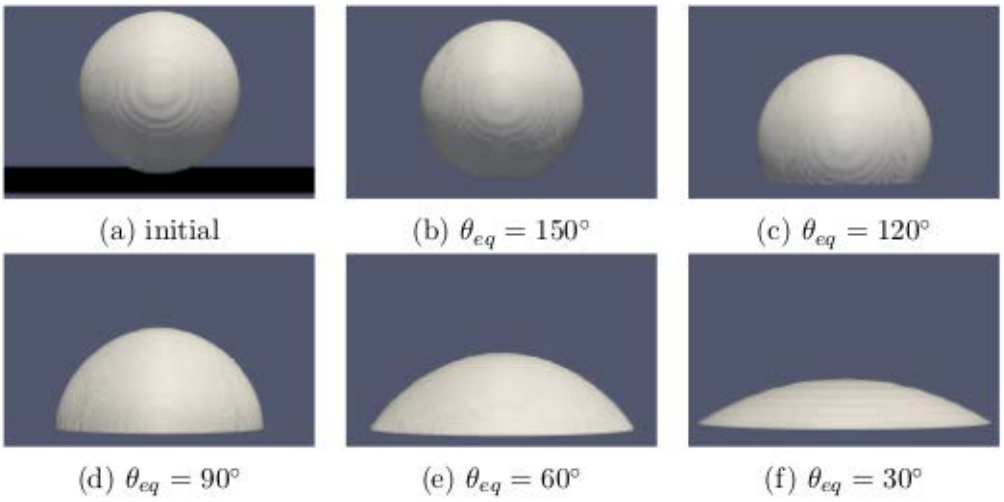

Figure 1. Equilibrium shape of a water droplet on a plane wall at different values of θ_{eq}.

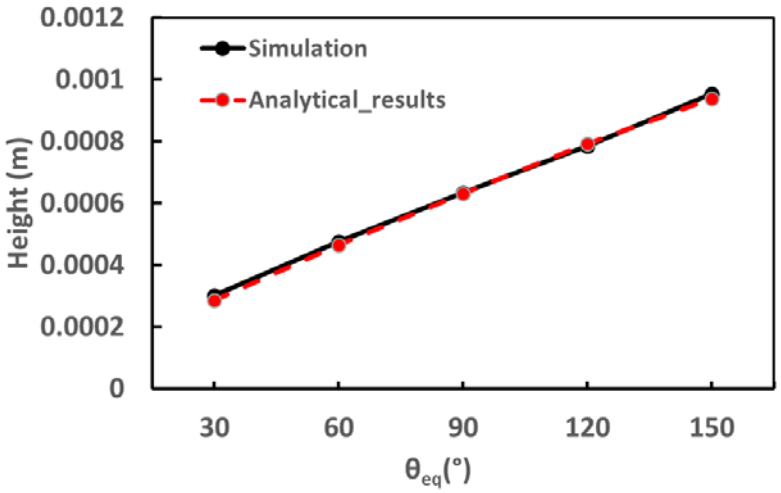

Figure 2. Comparison of the droplet height between analytical solutions and simulation results for static equilibrium of a water droplet on a plane wall at different contact angles.

3.2 Droplet-sphere contact

Another verification is chosen as the case of a droplet adhering to a spherical particle, which was also reported in the work of Suh and Son [19]. Again, no gravity is considered, the droplet is therefore subjected to viscosity, inertia and surface tension including wall adhesion (via Eq. (9) with a given θ_{eq}). Initially, a spherical droplet is placed just touching to the top of a stationary particle with the same size as the droplet, as depicted in Figure 3(a). The parameters for the simulations are listed in Table 2. The resolution is kept the same for all the simulations, i.e., 20 grid cells per initial droplet diameter. Simulations were performed for different values of the equilibrium contact angle θ_{eq},

resolving the transient motion of the droplet towards a steady state. Assuming that the droplet shape at equilibrium is a truncated sphere, the deformed droplet can be determined analytically for given values of θ_{eq} and initial diameter (detailed in [19]). Figure 3(b)-(f) compares the droplet shape (plotted in a 2D cross section) obtained from simulations with the analytical solutions. A very good agreement is achieved for all the considered contact angles.

Table 2. Parameters used in simulation of droplet-sphere contact.

Parameters	Values	Units
Liquid density ρ_l	1070	kg/m^3
Liquid viscosity μ_l	0.0036	Pa·s
Surface tension coefficient σ	0.04	N/m
Gas density ρ_g	1.2	kg/m^3
Gas viscosity μ_g	1.8E-5	Pa·s
Droplet initial diameter	5E-5	m

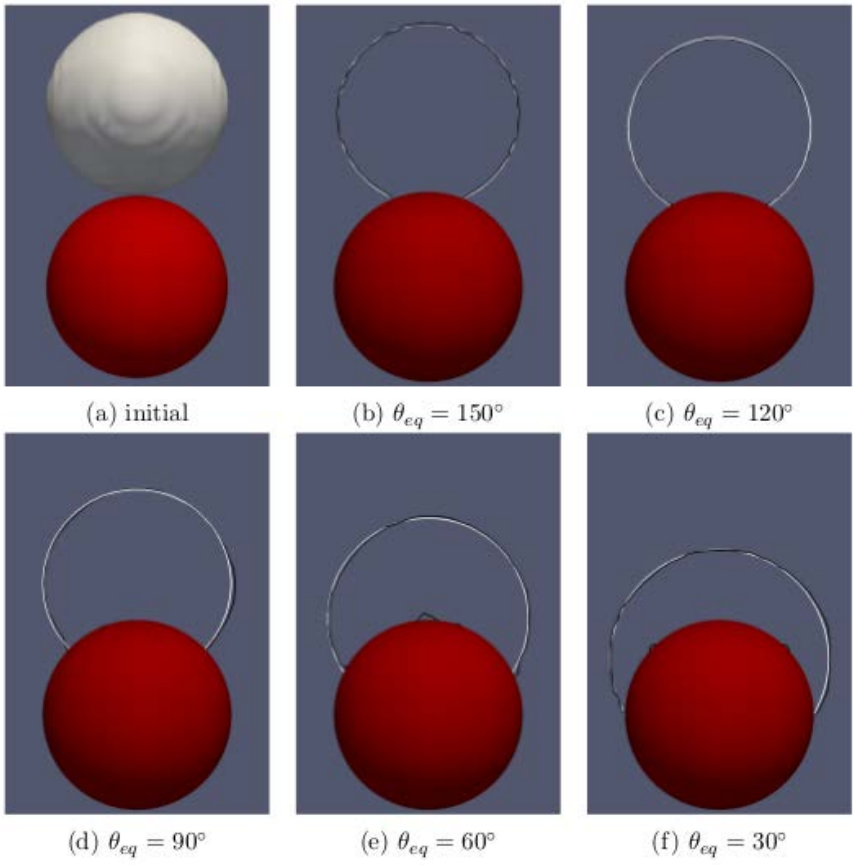

Figure 3. Static equilibrium of a liquid droplet adhering to a sphere at different contact angles. The red sphere represents the stationary particle, the black line indicates the 2D outline (at the centre plane) of the droplet from simulation results, and the white line shows the analytical solution.

3. RESULTS

After detailed verification of our model, in this section, we will present the results for normal impacts of a spherical glass particle on a flat glass plate covered by a thin layer of water. Table 3 gives the relevant parameters used for the considered problem. No-slip boundary conditions are imposed at the surface of the particle as well as at the bottom wall. Free slip conditions are used at the side boundaries confining the computational domain in the lateral directions, while a constant pressure outflow condition is used for the top boundary. The particle is released from its initial position just above the liquid layer at t=0 s with a specified (input) velocity. For the calculation of the wet restitution coefficient, the impact velocity and the rebound velocity are defined as: v_{im} is taken at the moment when the particle just touches the liquid, whereas v_R is taken as the particle velocity when the rupture of the liquid bridge takes place. Different contact angles are used when the particle moves downwards and upwards, respectively. These values of θ_{eq} are chosen from the data of the contact angle, which were measured from different experiments of normal impact.

Table 3. Parameters used in simulation of a sphere impacting on a wet surface.

Parameters	Values	Units
Liquid density ρ_l	1000	kg/m^3
Liquid viscosity μ_l	0.001	Pa·s
Liquid layer thickness δ_l	4E-4	m
Surface tension coefficient σ	0.0728	N/m
Gas density ρ_g	1.2	kg/m^3
Gas viscosity μ_g	1.8E-5	Pa·s
Particle density ρ_p	2526	kg/m^3
Particle diameter d_p	0.00174	m
Dry restitution coefficient	0.96	-
Gravity (z-dir)	-9.81	m/s^2
Computational domain (x-, y-, z-dir)	$3d_p \times 3d_p \times 4d_p$	-
θ_{eq} for particle penetration	150	°
θ_{eq} for particle rebound	15	°

First, a grid sensitivity study was carried out for an impact velocity v_{im}=1.13 m/s. The simulation results of the wet restitution coefficient are shown in Table 4 at four different grid resolutions. The obtained e_{wet} shows a slight decrease as the grids are refined, implying only a weak grid sensitivity. This is expected because of the following reasons: 1) regarding the computation of the drag force, the current IB method has been demonstrated by Deen et al. [16] to be less grid-dependent but more

accurate than conventional IB methods that require calibration of the particle diameter. 2) During the collision process, the free interface formed around the surface of the particle possesses a curvature roughly equivalent to the particle size. This leads to a relatively same grid resolution as d_p/h for the modelling of the free interface in VOF, which is sufficiently high even for the coarsest grids considered in this study. Therefore, finer grids were not considered in this work, as they introduce an excessive computational load and an extremely small time step.

Table 4. Grid sensitivity: simulation results of e_{wet} at different grid resolutions

δ_l/h	8	10	12	15
d_p/h	34.8	43.5	52.2	65.3
e_{wet}	0.584	0.563	0.557	0.553

The downward velocities of the sphere are plotted versus time in Figure 4. The velocity history obtained from the simulation at a resolution of $d_p/h = 12$ is compared with the velocity experimentally observed, showing a very good agreement. The slight deviation of the details before t=2.2 ms can be explained by imperfection of the experimental measurement as illustrated in Crüger et al [20]. The main imperfection causing this deviation originates from the part of the particle that is immersed in the liquid, where the boundary of the particle is hard to identify from the recorded images. On the contrary, numerical modelling has the advantage that the impact velocity and the rebound velocity can be exactly captured, as marked in Figure 4. This is however not the case for the experimental measurements, from which the two velocities are taken as mean values of the particle velocities obtained before impact and after rupture of the liquid bridge, as explained in Fig. 2 in [20]. Nevertheless, Figure 4 shows that the obtained v_{im} and v_R are consistent between the simulation and the experiment, resulting in the same wet restitution coefficient.

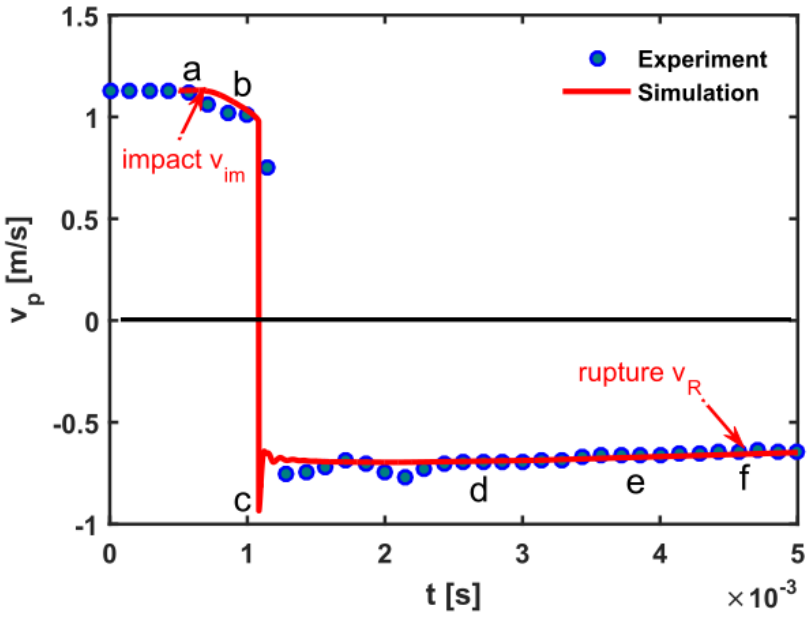

Figure 4: Simulation results and experimental measurements of velocity history of a spherical particle (1.74 mm) colliding with a 400 µm liquid layer at an impact velocity of 1.13 m/s. The arrows indicate where the v_{im} and v_R are captured from simulation results. Letters (a-e) are related to the corresponding snapshots shown in Figure 5.

A series of snapshots during the collision process are shown in Figure 5, from simulation results as well as high-speed recording experiments. Both simulation snapshots and experimental images clearly present four intervals during the full period of the collision that have been reported by many researchers (e.g., [3]): penetration of particle into liquid layer (a-b-c), contact with the wall (c), emergence of particle (c-d), as well as formation (e) and rupture (f) of the liquid bridge. During the penetration of the particle into the liquid layer, the liquid beneath the particle is squeezed out of the contact area. After the contact of the particle and the wall, liquid at the sides quickly moves backwards to the particle. A liquid bridge is then formed, which becomes thinner during rebound of the particle. Eventually, the liquid ruptures when the particle kinetic energy is larger than the bridge rupture energy. Furthermore, this figure shows that the height (about $2.5d_p$) of the formed liquid bridge predicted by the simulation agrees quite well with that observed from the experiment. This is considered as a significant improvement in comparison to the results reported in Jain et al. [11], where almost no liquid bridge could be observed. This improvement is mainly a result of the incorporation of the contact line model described earlier, which takes into account the modelling of the gas-liquid-solid contact line and the wetting of the particle. Furthermore, the use of the actual contact angles that are directly measured from the referenced experiments significantly improves the prediction of the dynamics of the liquid bridge in simulations.

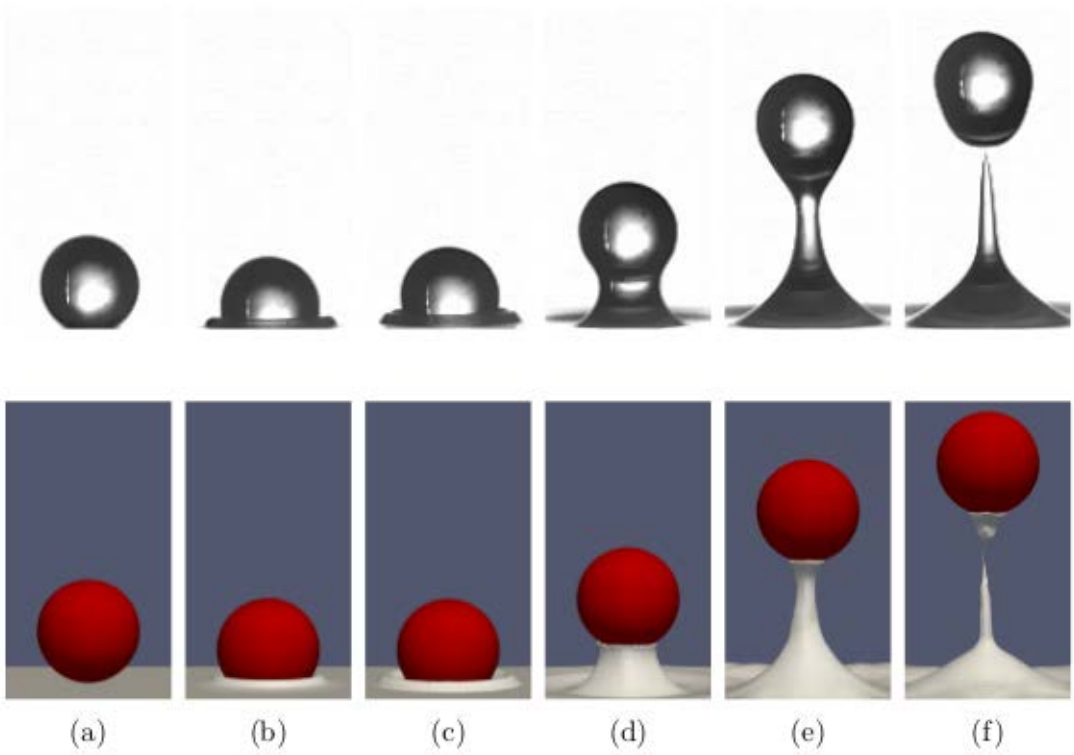

Figure 5: Snapshot sequence of a spherical particle (1.74 mm) impacting on a wet plate covered with 400 µm liquid layer at an impact velocity of 1.13 m/s: experimental high-speed recording images (top) and simulation results (bottom).

Finally, the influence of liquid viscosity on the wet restitution coefficient is investigated, while keeping the other parameters the same as shown in Table 3. Viscous dissipation is one of the major contributions to energy absorption during penetration and rebound of the particle [3,4,5]. Figure 6 plots the wet restitution coefficient e_{wet} as a function of liquid viscosity μ_l for a 1.74 mm sphere impacting on a 400 µm liquid layer at an impact velocity of v_{im}=1.0 m/s. Different liquid viscosities are considered, ranging from a low viscosity (1.0 mPa·s) to a high viscosity (17.5 mPa·s). Simulation results are compared to the experimental average data with error bars implying strong experimental scatter. An excellent agreement can be observed between the simulation and experimental results. In

addition, it is also observed that e_{wet} decreases linearly with increasing liquid viscosity. This observation can be understood from the fact that the viscous dissipation, which contributes most to the energy dissipation, arises during particle movement in the liquid due to the liquid shear flow between the particle and the plate. This viscous force is linearly proportional to the liquid viscosity. Consequently, if other parameters are kept constant, the restitution coefficient would also be expected to linearly change with the liquid viscosity as illustrated by the results shown in Figure 6. In addition, Figure 7 plots the particle velocity histories computed from the simulations. All the trajectories show a similar trend as that in Figure 4. It is seen that the viscous effect by different liquid viscosities leads to a clear difference of the particle velocity during bouncing back from the wall, whereas only a slight change of the particle velocity during penetration.

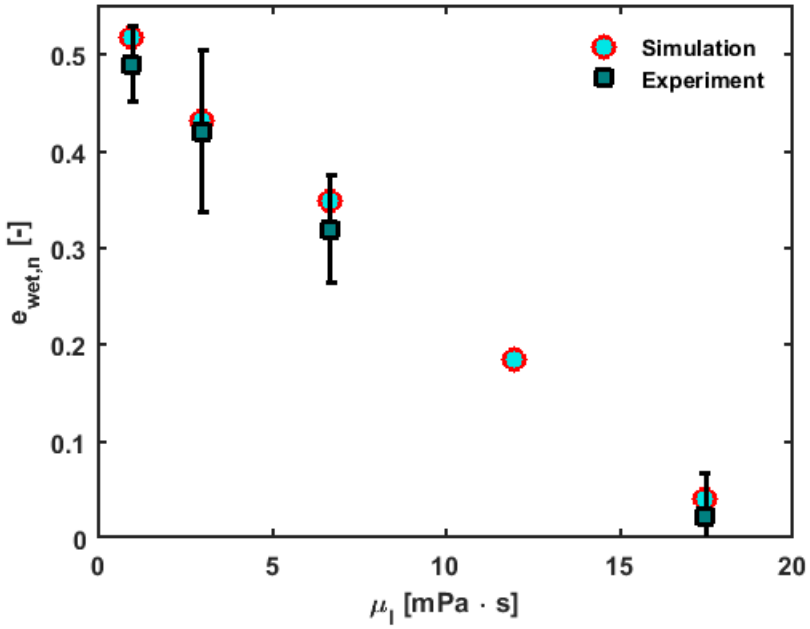

Figure 6: Wet restitution coefficient as a function of liquid viscosity for a spherical particle impacting on a 400 µm liquid layer at an impact velocity of 1.0 m/s: simulation results and experimental average data with standard deviations.

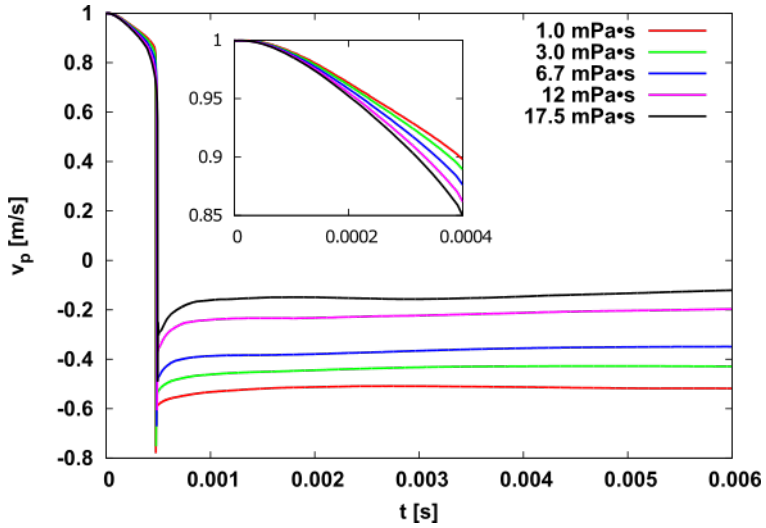

Figure 7: Velocity histories for a spherical particle impacting on a 400 µm liquid layer at an impact velocity of 1.0 m/s with different liquid viscosities.

4. CONCLUSIONS

In this paper, a numerical model is introduced to simulate the collision behaviour of a spherical particle on a wall surface covered by a thin liquid layer. The model combines a VOF method including the tensile force surface tension model, with a second-order implicit IBM. Besides, a contact model and a lubrication model are incorporated to model the wetting and lubrication, respectively. The implementation of the numerical model is verified by theoretical analysis of droplet-wall and droplet-sphere contacts.

Simulations are performed to study the normal collision of a sphere on wet surfaces, and the results are compared with experimental data. Detailed comparison has demonstrated the capability of our numerical model for qualitative as well as quantitative prediction of the collision dynamics in such systems. Simulations not only reproduce all the physical phenomena during the full collision period observed from experimental measurement, but also provide more (continuous) details for the impact period when large part of the particle is immersed in the liquid. The incorporation of the contact model significantly improves the prediction of the formation, thinning and rupture of the liquid bridge during impact. In addition, imperfections encountered in the experimental technique can be avoided in the numerical simulations. But meanwhile, we also need to keep in mind that for more accurate prediction of the simulations, some physical parameters (e.g. the contact angle) measured experimentally are very important.

LIST OF SYMBOLS

e_{wet}	wet restitution coefficient	
v_{im}	impact velocity	[m/s]
v_R	rebound velocity	[m/s]
ρ	density	[kg/m^3]
μ	viscosity	[Pa·s]
δ_l	layer thickness	[m]
θ_{eq}	equilibrium contact angle	[°]

ACKNOWLEDGEMENTS

We gratefully acknowledge for the financial support: Technology Foundation STW, The Netherlands, and German Research Foundation (DFG), Germany, with project number HE 4526/9-2.

REFERENCES

[1] M.S. Van Buijtenen, N.G. Deen, S. Heinrich, S. Antonyuk, J.A.M. Kuipers, A discrete element study of wet particle-particle interaction during granulation in a spout fluidized bed, Can. J. Chem. Eng., 87 (2009) 308-317.

[2] G.G. Joseph, R. Zenit, M.L. Hunt, A.M. Rosenwinkel, Particle-wall collisions in a viscous fluid, J. Fluid Mech., 433 (2001) 329-346.

[3] S. Antonyuk, S. Heinrich, N.G. Deen, J.A.M. Kuipers, Influence of liquid layers on energy absorption during particle impact, Particuology, 7 (2009) 245-259.

[4] R.H. Davis, D.A. Rager, B.T. Good, Elastohydrodynamic rebound of spheres from coated surfaces, J. Fluid Mech., 468 (2002) 107-119.

[5] V.S. Sutkar, N.G. Deen, J.T. Padding, J.A.M. Kuipers, V. Salikov, B. Crüger, S. Antonyuk, S. Heinrich, A novel approach to determine wet restitution coefficients through a unified correlation and energy analysis, AIChE J., 61 (2015) 769-779.

[6] A.A. Kantak, J.E. Galvin, D.J. Wildemuth, R.H. Davis, Low-velocity collisions of particles with a dry or wet wall, Microgravity - Science and Technology, 17 (2005) 18-25.

[7] F. Gollwitzer, I. Rehberg, C.A. Kruelle, K. Huang, Coefficient of restitution for wet particles, Physical Review E, 86 (2012) 011303.

[8] T. Müller, K. Huang, Influence of the liquid film thickness on the coefficient of restitution for wet particles, Physical Review E, 93 (2016) 042904.

[9] J. Ma, D. Liu, X. Chen, Experimental study of oblique impact between dry spheres and liquid layers, Physical Review E, 88 (2013) 033018.

[10] J. Ma, D. Liu, X. Chen, Normal and oblique impacts between smooth spheres and liquid layers: Liquid bridge and restitution coefficient, Powder Technol., 301 (2016) 747-759.

[11] D. Jain, N.G. Deen, J.A.M. Kuipers, S. Antonyuk, S. Heinrich, Direct numerical simulation of particle impact on thin liquid films using a combined volume of fluid and immersed boundary method, Chem. Eng. Sci., 69 (2012) 530-540.

[12] M. Wu, J. Khinast, S. Radl, A model to predict liquid bridge formation between wet particles based on direct numerical simulations, AIChE J., 62 (2016) 1877-1897.

[13] H. Kan, H. Nakamura, S. Watano, Numerical simulation of particle-particle adhesion by dynamic liquid bridge, Chem. Eng. Sci., 138 (2015) 607-615.

[14] D.L. Youngs, Time-dependent multi-material flow with large fluid distortion, in K.W. Morton, M.J. Baines (Eds.) Numerical Methods for Fluid Dynamics, Academic Press, New York, 1982, pp. 273-285.

[15] M.W. Baltussen, Bubbles on the cutting edge: direct numerical simulations of gas-liquid-solid three-phase flows, PhD thesis, in: Eindhoven University of Technology, NL, 2015.

[16] N.G. Deen, S.H.L. Kriebitzsch, M.A. van der Hoef, J.A.M. Kuipers, Direct numerical simulation of flow and heat transfer in dense fluid-particle systems, Chem. Eng. Sci., 81 (2012) 329-344.

[17] H. Brenner, The slow motion of a sphere through a viscous fluid towards a plane surface, Chem. Eng. Sci., 16 (1961) 242-251.

[18] M. Bellet, Implementation of surface tension with wall adhesion effects in a three-dimensional finite element model for fluid flow, Communications in Numerical Methods in Engineering, 17 (2001) 563-579.

[19] Y. Suh, G. Son, A sharp-interface level-set method for simulation of a piezoelectric inkjet process, Numerical Heat Transfer, Part B: Fundamentals, 55 (2009) 295-312.

[20] B. Crüger, V. Salikov, S. Heinrich, S. Antonyuk, V. Sutkar, N.G. Deen, J.A.M. Kuipers, Coefficient of restitution for particles impacting on wet surfaces: An improved experimental approach, Particuology, 25 (2016) 1-9.